Cylindrical Elastic Crawler Mechanism for Pipe Inspection Inspired by Amoeba Locomotion*

Fumika Fukunaga and Jun-ya Nagase, *Member, IEEE*

***Abstract*— The diverse pipe installations used today include pipelines in chemical plants, water pipes, and gas pipes. Severe accidents at such pipe installations must be prevented by regular pipe inspection and repair. As described herein, a novel tracked crawler mechanism is proposed for pipe inspection. This simple and compact cylindrical elastic tracked crawler has multiple crawler belts in axial symmetry to a cylindrical frame, driven solely by a single motor via a single worm. It is suitable for propulsion through a narrow pipe. It can propel itself upward in a pipe using elastic force generated by deforming the crawler belt passively. Moreover, the proposed tracked crawler can cross over a level difference and pass an elbow by deforming the crawler belt passively along the pipe shape. For a prototype tracked crawler, running performance experiments conducted in various pipe conditions yielded good results. This study clarified the relation between belt rigidity and traction force in theory and experiment respectively.**

I. Introduction

Many pipe-inspection robots have been developed to date, including wheel robots, snake-like robots, peristaltic crawling robots, and tracked crawler robots. All these robots have high running performance in pipes, but they entail some important pipe-propulsion difficulties related to their complicated structure and propulsion mechanisms. For instance, wheel robots [1] can pass a level difference and an L-shaped pipe using sensors, some actuators, and link mechanisms. However, reducing the size of such robots is difficult because of their complicated structures. Snake-like robots [2] can pass level differences and can run upward in vertical pipes by controlling some joints that have numerous degrees of freedom. However, slippage between the body and the pipe occurs when the gliding angle is low. The gliding angle is low when the robots run in a narrow pipe. Therefore, it is difficult to propel a robot effectively in such a pipe. Peristaltic crawling robots [3]–[4] are also proposed. These robots can propel themselves even in a narrow pipe by generating regressive waves independently. However, the adequate cycle of the regressive wave depends on the pipe diameter. Moreover, if the regressive wave cycle is fast, then the moving efficiency of the robots decreases greatly because of slippage in the pipe.

To meet difficult demands for these devices, tracked crawler robots [5]–[7] have been developed. Actual pipe installations have numerous uneven surfaces inside pipes such as level differences at fittings, connectors, and elbows. Tracked crawler robots are suitable for such uneven ground conditions because they can travel by traversing uneven ground flexibly with a crawler belt attached to the ground surface in conditions that afford a large ground contact area. However, it is also difficult to reduce the size of these tracked crawler robots because of complicated structures and many actuators. For instance, they need sliding-mechanisms, actuators, and sensors to control the robot size to conform to the pipe diameter [6]. Furthermore, they have articulating mechanisms and actuators for navigation in the pipe [7]. Therefore, they are unsuitable for propulsion in narrow pipes.

In this study, we therefore aimed at implementation of a tracked crawler robot for pipe inspection with high running performance in vertical, corner, and uneven narrow pipes. We have so far been developed cylindrical tracked crawler robot inspired by amoeba locomotion [8]. The tracked crawler mechanism propels the robot by driving multiple crawler belts in axial symmetry to a cylindrical frame with a single actuator via a single worm. Consequently, it is an extremely simple structure compared to conventional tracked crawler with complicated structures and many actuators [9]–[10]. However, such a previous type [8] cannot propel itself upward. It cannot accommodate level differences such as fittings and L-shaped corners such as elbow.

Herein, we propose an elastic tracked crawler mechanism for pipe inspection. The crawler belts of this mechanism have elasticity and are bent outward, enabling it to propel itself upward inside a pipe using elastic force of the crawler belt, as presented in Fig. 1(a). Red arrow and yellow arrow describe elastic force and travel direction respectively. Moreover, it can traverse a level difference such as a fitting and can pass through an elbow L-shaped corner by deforming the elastic crawler belt passively along the pipe shape, as presented in Fig. 1(b) and (c). This report describes the structure, driving principle and prototype evaluation of the proposed cylindrical crawler robot.

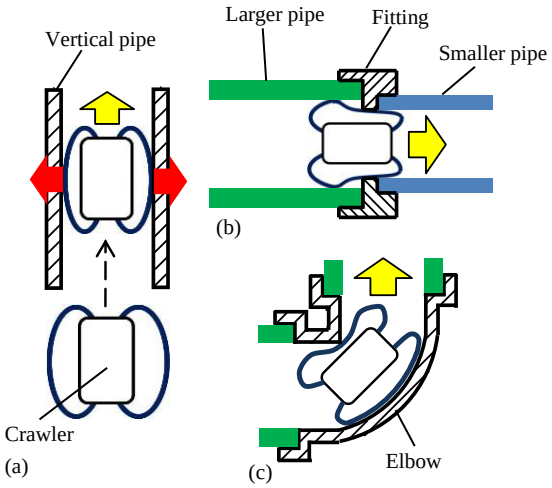

Figure 1. Propelling in pipes using the elastic crawler belt: (a) vertical pipe, (b) different-diameter pipe, and (c) elbow.

*Research supported by Grant-in-Aid for Young Scientists (B) (No. 26750172).

Fumika Fukunaga and Jun-ya Nagase are with Mechanical and Systems Engineering, Science and Technology, Ryukoku University, Shiga, Japan (e-mail: nagase@rins.ryukoku.ac.jp).

II. STRUCTURE

Fig. 2 portrays the basic structure of an amoeba and its locomotion mechanism. An amoeba, a single-celled creature, consists mainly of endoplasm, ectoplasm, and a pseudopod. Its locomotion mechanism [11] is the following. First, endoplasm flows forward inside the ectoplasmic tube. Then the amoeba advances by protruding the pseudopod outward from the body. Fig. 3 shows a structural drawing of the proposed tracked crawler mechanism. This mechanism is a cylindrical crawler unit comprising a single geared motor, silicone rubber crawler belts, a single worm, and a resin frame. Six crawler belts are spaced at equal intervals around the longitudinal axis of the cylindrical frame. Each crawler belt is wound around the frame: both ends are connected, producing a loop. Also, teeth having a rake angle corresponding to the lead angle of the worm tooth are formed on the crawler belt outer surface. The geared motor is mounted as stationary inside and coaxially to the frame. The worm, which is attached to the motor shaft, is positioned to engage with each of the six crawler belts.

Regarding the driving principle, first, the motor fixed to the frame creates rotation via the gear. Then the rotating worm engages with all six crawler belts to propel the crawler robot in the longitudinal direction. The crawler moves forward by this mechanism. Moreover, inverse rotation of the motor produces backward movement. This simple and compact cylindrical tracked crawler has multiple crawler belts in axial symmetry to a cylindrical frame, driven only by a single motor via a single worm. It is suitable for travelling in confined spaces such as in a narrow pipe.

Features of this cylindrical tracked-crawler mechanism are the following.

(i) The worm track mechanism drives the simple structure, facilitating considerable size reduction compared to the conventional cylindrical crawler structure. Therefore, it is suitable for movement through confined spaces such as narrow pipes.

(ii) It is operable even when top–bottom or left–right sides of the robot contact walls simultaneously by virtue of its multiple crawler belts in axial symmetry.

(iii) The proposed tracked-crawler can propel itself upward in a pipe using the elastic force of the crawler belt.

(iv) It can traverse a level difference and pass an elbow by deforming the crawler belt passively along the pipe shape.

III. DESIGN

This chapter presents descriptions of the proposed tracked-crawler design.

A. *Frame size, worm size, and belt width*

First, dimensioning to radial direction of the proposed tracked-crawler is described. Each size is determined geometrically based on the inner diameter of the pipe in which it moves. Fig. 4 depicts a schematic diagram of the proposed tracked-crawler in an axial view of the time it propels inside a minimum-diameter pipe. From Fig. 4, the inner radius of the pipe is *R*. Each size calculated based on *R* is the frame outer radius *R*', the crawler belt width *b*, the frame groove width *b*', the worm tip radius *r*, and the worm root radius *r*'. As shown in Fig. 4, the outer radius of the frame *R*' is

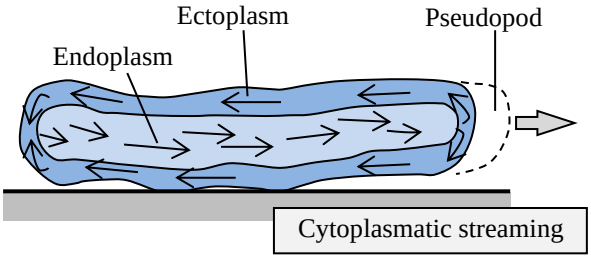

Figure. 2. Structure and locomotion mechanism of amoeba.

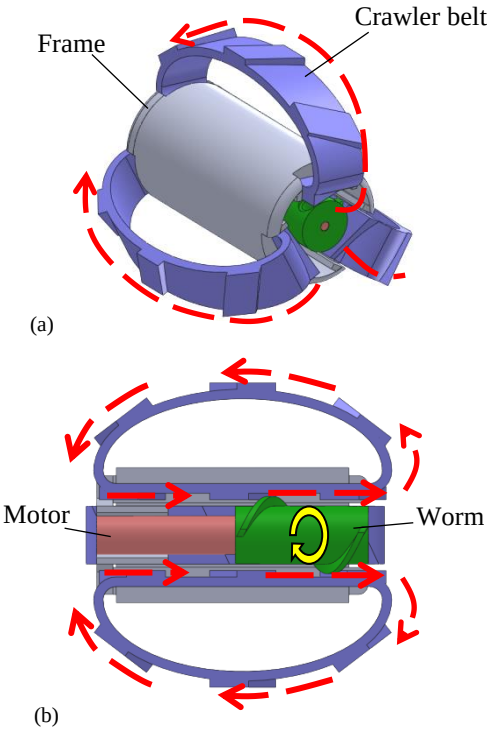

Figure 3. Structure of proposed cylindrical elastic tracked-crawler mechanism: (a) overview and (b) section.

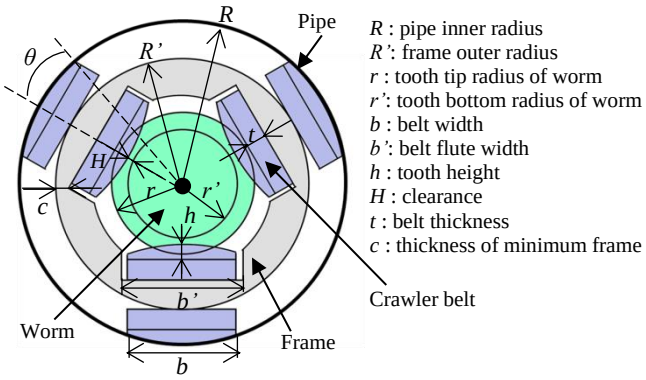

Figure 4. Schematic diagram of the proposed robot in an axial view

obtained using the pipe inner radius *R*, tooth depth *h*, and the belt thickness *t*, as in the following equation.

$$R' = R - (h + t) \tag{1}$$

Therein, θ denotes the angle between the straight line that links the worm center to the corner of the tooth tip, and the

perpendicular bisector of the crawler belt width *b*. Also, n is number of the crawler belt. It must satisfy following equation.

$$\theta \le \frac{\pi}{n} \tag{2}$$

The crawler belt width *b* is calculable using the radius of the inside the pipe as in the following equation.

$$b = 2R\sin\theta \tag{3}$$

where *H* is the clearance between the frame groove side and the belt side. The worm tip radius *r* is derived as

$$r = \sqrt{(R' - c)^2 - \left(\frac{b'}{2}\right)^2} - t, \tag{4}$$

where *c* denotes the minimum frame thickness, *b*' denotes the frame groove width. The worm root radius *r*' is derived as shown below.

$$r' = r - (h + H) \tag{5}$$

In that equation, *H* denotes the clearance between the belt tooth tip and the worm tooth bottom. The belt tooth depth *h*, the belt thickness *t*, the clearance between the belt tooth tip and the worm tooth bottom *H*, and the minimum thickness of the frame *c* respectively depend on the elastic force of the belt or the friction force between the belt toothing and the worm toothing or the frame strength.

For this study, pipes of two different inner diameters are used. Their minimum diameter is 28 mm, corresponding to a 25A pipe. Therefore 25A was used in the design. The frame outer radius *R*', the crawler belt width *b*, the frame groove width *b*', the worm tip radius *r*, and worm root radius *r*' are calculated respectively as 10.5 mm, 9.0 mm, 10.0 mm, 6.0 mm, and 4.5 mm based on *R* set as 14 mm.

B. Frame length

Next, the setting of dimensions to the longitudinal direction of the proposed tracked-crawler is described. For this study, each longitudinal dimension is designed geometrically based on each dimension of an elbow in which the crawler robot moves. Fig. 5 depicts a schematic diagram of the elbow and the crawler. The tracked-crawler shown in that figure is in a state where the robot crawler belt is deformed to the inside maximally. The equation to derive the longitudinal maximum length of the robot depends on the outer diameter of the tracked-crawler *d*. Therein, *o* denotes a middle point of the minimum circular arc of inside the elbow; *c* denotes a middle point of a straight line that links point p to point q in the maximum circular arc $\overline{pq}$. Now, in case the outer diameter of the crawler *d* is shorter than that of straight line that links point *o* to point *c* $\overline{oc}$, the following equation can be derived.

For this study, the inner diameter of the elbow *D* is selected as 40 mm, corresponding to 40A pipe, radius of curvature R_C is 20 mm, and tracked-crawler outer diameter *d* is 21 mm, calculated using the frame outer radius *R*', crawler belt tooth depth *h*, and belt thickness *t* determined in the previous section. In addition, (9) is applied to derive the

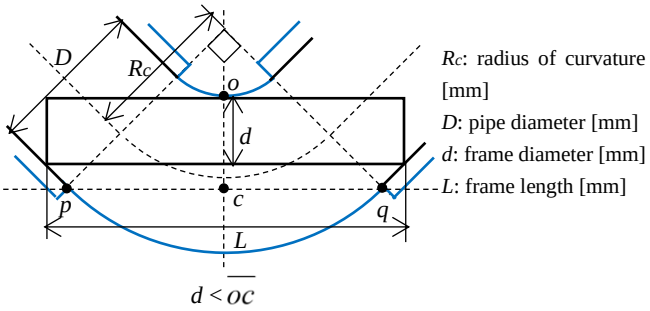

Figure. 5. Schematic diagram of the tracked-crawler inside an elbow.

$$0 < d < \frac{\sqrt{2}}{2}\left(R_c + \frac{D}{2}\right) - \left(R_c - \frac{D}{2}\right) \tag{6}$$

$$L < 2\sqrt{2}\left[\left(R_c + \frac{D}{2}\right) - \left\{\sqrt{2}\left(R_c - \frac{D}{2}\right) + \sqrt{2}d\right\}\right] + 2d + 2\left(R_c - \frac{D}{2}\right) \tag{7}$$

However, the following equation is obtainable for cases in which the crawler outer diameter *d* is longer than $\overline{oc}$.

$$\frac{\sqrt{2}}{2}\left(R_c + \frac{D}{2}\right) - \left(R_c - \frac{D}{2}\right) < d < D \tag{8}$$

$$L < 2\sqrt{\left(R_c + \frac{D}{2}\right)^2 - \left(d + R_c + \frac{D}{2}\right)^2} \tag{9}$$

longitudinal length of the robot because the outer diameter *d* satisfies (8). Based on the parameters described above, the longitudinal length of the robot *L* is determined as 42 mm.

IV. Prototype

Based on the design described above, a crawler unit was prototyped. The crawler belt production procedure, with mold forming of silicone rubber, is described first. Liquid rubber (KE-1600; Shin-Etsu Chemical Co. Ltd.) was poured into a mold, with a lid on. It was left untouched for 60 min in a 70°C thermostatic chamber. Then, after taking out the rubber fabricated by solidification, liquid rubber was applied to both ends, which were bonded and left untouched for 60 min in the thermostatic chamber again for complete adhesion. The crawler belt was finished. The frame and worm made of ABS resin were molded with a 3D printer (Dimension Elite; Stratasys Ltd.). The geared motor was a DC motor (GP13A SL; Maxon Motor AG).

Fig. 6 exhibits the prototype of the proposed tracked-crawler. Table 1 presents its specifications. The prototyped crawler has 42 mm total length and 18 g mass. The outer diameter of the maximally deformed crawler belt is 26 mm; the belt is 45 mm when not stressed by external forces.

V. Static Analysis of Traction Force

This chapter describes static analysis of the traction force of the proposed tracked crawler when it runs in a pipe. For this analysis, the crawler is assumed to run upward in the vertical pipe. The amounts of belt deformations are assumed to be equal to those when the tracked crawler moves in the pipe.

Fig.7 presents a schematic diagram of the tracked crawler moving upward inside the pipe. First, the longitudinal force F_W transmitted from the geared motor to the belt teeth through the worm is derived using the following equation.

$$F_W = \sum_{i=1}^{n} f_{Wi} = \frac{\tau_M}{r\tan(\beta+\lambda)} \tag{10}$$

In that equation, τ_M denotes torque of the motor, r denotes the worm pitch radius, β denotes the worm lead angle, and λ denotes the frictional angle between the worm tooth and the belt tooth. The driving force F_B of the crawler belt is derived using F_W as shown below.

$$F_B = \sum_{i=1}^{n} f_{Bi} = F_W - F_I \tag{11}$$

Therein, F_I stands for the frictional force acting on belts inside the tracked crawler. It is the sum of the frictional forces between the belt and the frame, and between the belt tooth bottom and worm tooth tip. It can be expressed as follows.

$$F_I = \sum_{i=1}^{n} f_{Ii} = n\mu_I Kx \tag{12}$$

In that equation, x denotes the amount of the belt deformation to the radial direction, μ_I stands for the frictional coefficient between the belt and the parts inside the tracked crawler, K signifies the nonlinear spring constant of the belt in the radial direction, and n represents the number of crawler belts. When the tracked crawler moves in the pipe, frictional force between the crawler belt and the pipe is generated in the belt in the opposite direction of the driving direction of the belt. The maximum frictional force F_O is

$$F_O = \sum_{i=1}^{n} f_{Oi} = n\mu_O Kx \tag{13}$$

In that equation, μ_O is the frictional coefficient between the belt and the pipe. The magnitude of the traction of the tracked crawler is proportional to that of the geared motor torque. However, it is less than the magnitude of the maximum frictional force of the belt. Therefore, the equation of the traction is divided into two cases as shown below. If the relation between the maximum frictional force F_O and F_B satisfies the following equation, then the traction F_T can be derived as shown in (15).

$$F_O < F_B + Mg \tag{14}$$

$$F_T = F_O - Mg \tag{15}$$

Therein, M stands for the mass of the tracked crawler. In addition, if the relation between the maximum frictional force F_O and the F_B satisfy following equation, then the traction F_T can be derived as (17).

$$F_O \geq F_B + Mg \tag{16}$$

$$F_T = F_B - Mg \tag{17}$$

Based on the equations from (14) to (17), the relation between the spring constant of crawler belts K and the traction F_T is discussed as follows: First, we specifically examine when the relation between F_O and F_B satisfy (14). In this case, the magnitude of the traction F_T is the difference between the maximum frictional force F_O and the gravity acting on the tracked crawler Mg, as described in an (15). The maximum frictional force F_O is proportional to the spring constant K, as described in (13). Therefore, traction F_T increases concomitantly with increasing the spring constant K, when (14) is satisfied.

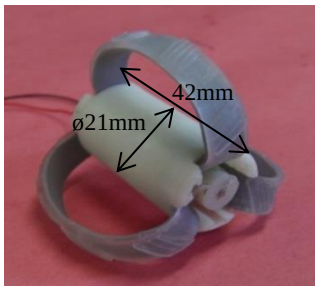

Figure. 6 A photograph of a prototyped tracked-crawler.

TABLE I SPECIFICATIONS OF PROTOTYPE TRACKED-CRAWLER

Frame length		42 mm
Frame diameter		ø21 mm
Pipe that can be run	Horizontal pipe	More than ø 28 mm
	Vertical pipe	From ø 28 mm to ø 40 mm
Weight		18g
Motor		RE6 0.3W 221:1, Maxon motor
Pitch of worm gear		18.4 mm
Lead angle of worm gear		29.2 deg
Crawler belt		
	Number	3
	Material	silicone rubber
	Width	9 mm
	Height of belt part	1.5 mm
	Height of tooth part	1 mm

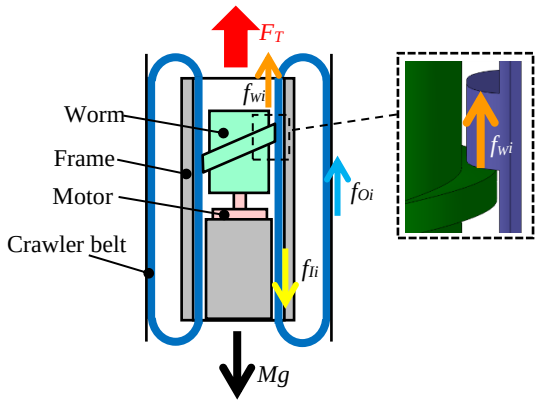

Figure 7. Schematic diagram of the tracked-crawler that propels upward inside the pipe.

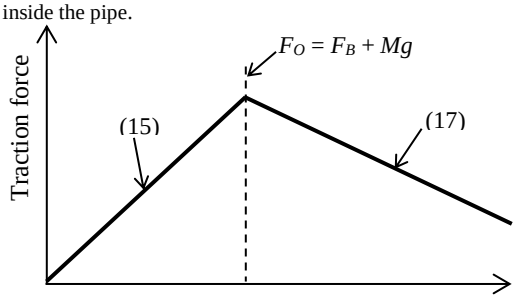

Figure 8. A relationship between the spring constant of the crawler belt and the traction force of the tracked crawler in this study.

When the spring constant K is higher, the maximum frictional force F_O exceeds the driving force of belt F_B. At this time, the relation between the driving force of the belt F_B and the maximum frictional force of that F_O is changed to (16) from (14). In this case, traction F_T decreases when the driving force of belt F_B decreases by (17). Also, (11) and (12) show that the F_B decreases concomitantly with increasing the spring constant of the belt K because the internal frictional force F_I increases. Therefore, traction F_T decreases concomitantly with increasing the spring constant of the belt K when (16) is satisfied.

The following is a summary of the explanation above. If the relation between F_O and F_B satisfies (14), then traction F_T increases when the spring constant of the belt K increases. If the relation between F_O and F_B satisfies (16), traction F_T decreases when the spring constant of the belt K increases. Furthermore, when the sum of the belt driving force F_B and the gravity Mg is equal to the maximum frictional force F_O, traction force F_T reaches its maximum value. Fig. 8 depicts the qualitative relationship between the spring constant of the belt K and the traction force F_T based on the static analysis described above.

VI. Experiments

A. Relation between belt hardness and traction force

This section presents a description of the basic characteristics of the prototyped tracked crawler. First, the relation between the rubber hardness (durometer shore A) of belts and the traction force was examined using experiments. This experiment uses six tracked crawlers with different rubber hardness of belts. The respective rubber hardness of durometer shore A was 30, 40, 50, 60, 70 and 80: young's modulus increases when durometer shore A increases in generally. The experimental setup is presented in Fig. 9. One end of a string was connected to the crawler. Another end was connected to a force gage (FGP-5; Nidec Corp.) fixed to the ground. Then the crawler traction force was measured by the force gage of the crawler in a vertical pipe. The pipe diameter was 28 mm.

Fig. 10 depicts experimentally obtained results showing the traction force for tracked crawlers with many or fewer crawler belts. The maximum value of the traction force was found for 60 belts: 2.0 N.

Next, the relation between the rubber hardness of the belts and the traction force is discussed. For 60 or lower belts, the traction force increased concomitantly with increasing rubber hardness of the belts. This result is qualitatively consistent with (15). Additionally, results show that the belts slipped against the pipe in this experiment system. This is equivalent to (14). Consequently, results clarified that the traction force increases concomitantly with increasing rubber hardness of the belts when the maximum frictional force of the belts is less than the sum of the driving force of the belts and the gravity of the crawler, such as when the rubber hardness is low. However, when 60 or more belts were used, the traction force decreased concomitantly with increasing rubber hardness of the belts. This result is qualitatively consistent with (17). Also, results show that the belts did not slip against the pipe when 70 and 80 belts were used. This is equivalent to (16). Therefore, the traction force decreases concomitantly with increasing rubber hardness of belts when the maximum frictional force of the belts is greater than the sum of the driving force of the belts and the gravity of the crawler, such as when the rubber hardness of the belts is large.

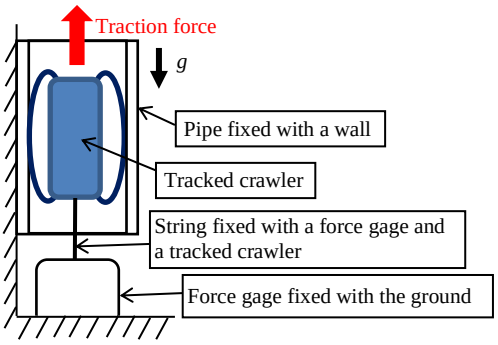

Figure 9. Experimental system for the measurement of traction force.

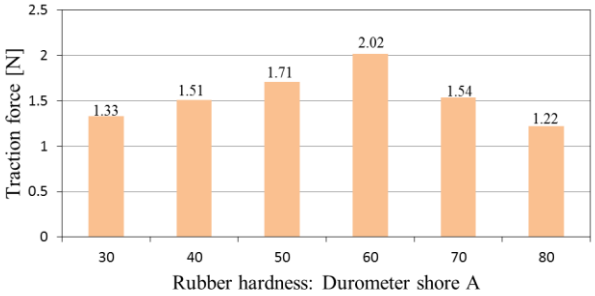

Figure 10. Experimental result of traction forces of the tracked crawler on each rubber hardness (durometer shore A) of the crawler belts.

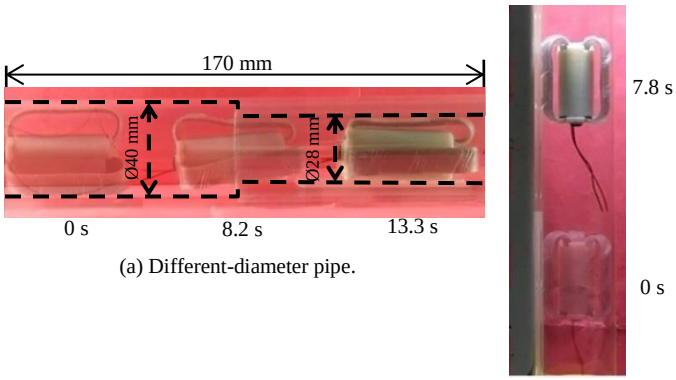

(a) Different-diameter pipe.

(b) Vertical pipe

(c) Elbow

Figure 11. Running experiments in a different diameter pipe, vertical pipe and elbow.

B. Running experiments in pipes

This section explains the prototype tracked crawler running performance. This experiment examined its adaptability to different pipe diameters. Furthermore, its through a vertical pipe and an elbow were examined. In this experiment, the tracked crawler whose rubber hardness of

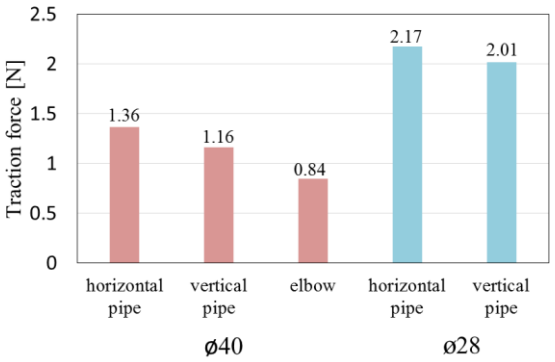

Figure 12. Experimental result of traction forces of the tracked crawler on each pipe: horizontal, vertical and elbow of ø40; horizontal and vertical of ø28

belts was 60 was used. Acrylic resin pipes were used in each experiment.

First, running experiments were done with different diameter pipes. For this experiment, the inner diameter of the larger diameter pipe was 40 mm. That of the narrower pipe was 28 mm. The crawler velocity was set as 20 mm/s. Figure 11(a) presents photographs showing the crawler movement in pipes of different diameters. The tracked crawler moved to the ø40 mm pipe from the ø28 mm pipe. Results show that the crawler traverses the level difference by deforming the crawler belt passively along the pipe shape. Figure 11(b) depicts photographs showing the tracked crawler moving in the vertical pipe. Therein, the crawler belt velocity was set to 20 mm/s. Results of experiments show that the tracked crawler can move upward while holding itself to the pipe by the elastic force of the crawler belt in the vertical pipe. This experiment clarified that the proposed tracked crawler requires no sensors or complicated structures in such pipes. Next, tracked crawler prototype running experiments were conducted in an elbow with 40 mm inner diameter. Figure 11(c) shows photographs showing the crawler robot moving in an elbow. Experiment results confirmed that it can also move in the elbow by deforming the crawler belts along the curving pipe surface.

C. Traction force in each pipe

This section describes traction force of the tracked crawler in various pipes. Fig. 12 shows the traction force of the crawler in the horizontal pipe, the vertical pipe, and the elbow of ø40 mm, and in the horizontal pipe and the vertical pipe of ø28 mm. For inner diameter 28 mm pipe, traction force in the vertical pipe is smaller 0.15 N than that in the horizontal pipe. For inner diameter 40 mm pipe, the traction force in the vertical pipe is smaller 0.2 N than that in the horizontal pipe. The gravity of the crawler is 0.17 N. Therefore, these results indicate that the gravity decreases traction force of the crawler in the vertical pipe, as shown in (15).

Traction force in ø28 mm pipe is larger than that in ø40 mm pipe. When the amount of belts deformation is larger, the elastic force of belts becomes large. Also, frictional coefficient between the belt and the pipe in ø28 mm is higher than that in ø40 mm, because the contact area of the belts and the pipe in ø28 mm is larger than that in ø40 mm. These results indicate that because both the frictional coefficient and the elastic force of the belts were increased, traction force increased concomitantly with decreasing the pipe inner diameter, as described in (13) and (15).

Traction force of the crawler in an elbow of ø40 mm was the smallest of all pipes. The curvature radius of inside wall is smaller than that of outside wall. As mentioned above, results shows that because frictional coefficient between the belt and the inside wall is smaller than that in the straight pipe, the traction force in elbow was smaller than that in the straight pipe.

VII. Conclusion and Future Work

As described in this paper, we proposed a novel tracked crawler mechanism for running inside narrow pipes. In this study, the qualitative relation between the rubber hardness of the crawler belts and the traction force was demonstrated using theoretical analysis and experimentation. Furthermore, performances of the prototyped crawler robot were evaluated experimentally. Experiments verified that a prototyped tracked crawler can move in a horizontal pipe, vertical pipe, in a pipe with level differences, and even in an elbow.

However, the moving direction of that presented herein cannot be controlled. Therefore, future developments will be planned to make a crawler waterproof, produce a steering mechanism and load a camera with a crawler in order to run the robot in pipe underwater, control the travelling direction and operation check in pipe inspection.

References

[1] E. Dertien, S. Stramigioli and K. Pulles, “Development of an inspection robot for small diameter gas distribution mains,” *Proc. 2011 IEEE International Conference on Robotics & Automation*, China, 2011. pp. 5044-5049

[2] S. Wakimoto, K. Suzumori, M. Takata and J. Nakajima, “In-Pipe Inspection Micro Robot Adaptable to Changes in Pipe Diameter,” *Journal of Robotics and Mechatronics*, Vol. 15, No. 6, pp. 609-615, Dec, 2003.

[3] S. Horii and T. Nakamura, “An In-Pipe Mobile Robot for Use as an Industrial Endoscope Based on an Earthworm's Peristaltic Crawling,” *Journal of Robotics and Mechatronics*, Vol. 24, No. 6, pp. 1054-1062, Dec, 2012.

[4] N. Saga and T. Nakamura, “Elucidation of propulsive force of micro-robot using magnetic fluid,” *Journal of Applied Physics*, Vol. 91, No. 10, pp. 7003-3005, May, 2003.

[5] J. Prak, D. Hyun, W. Cho, T. Kim and H. Yang, “Normal-Force Control for an In-Pipe Robot According to the Inclination of Pipelines,” *IEEE Tans. Industrial Electronics*, Vol. 91, No. 10, pp. 7003-3005, May, 2003.

[6] M. Muramatsu and Y. Suga, “Autonomous Mobile Robot System for Monitoring and Control Penetration during Fixed Pipes Welding,” *JSME International Journal*, Vol. 46, No. 3, pp. 391-397, Jun, 2003.

[7] J. Borenstein, M. Hansen and A. Borrell, “The OmniTread OT-4 Serpentine Robot – Design and Performance,” *Journal of Field Robotics*, Vol. 24, No. 7, pp. 601-621, Jul, 2007.

[8] J. Nagase, K. Suzumori and N. Saga, “Development of Worm-Rack Driven Cylindrical Crawler Unit,” *Journal of Advanced Mechanical Design, Systems, and Manufacturing*, Vol. 7, No. 3, pp.422-431, May, 2013.

[9] G. Lan, S. Ma, K. Inoue and Y. Hamamatsu, “Development of a novel crawler mechanism with polymorphic locomotion,” *Advanced Robotics*, vol. 21, No. 3-4, pp. 421-440, 2007.

[10] K. Tadakuma, R. Tadakuma, K. Nagatani, K. Yoshida, A. Ming ,M. Shimojo and K. Iagnemma, “Basic Running Test of the Cylindrical Tracked Vehicle with Sideways Mobility,” in *Proc. 2009 IEEE/RSJ International Conference on Intelligent Robots and Systems*, USA, 2009, pp. 1679-1684.

[11] J.M. Lackie, *Cell Movement and Cell Behavior*, London: Allen and Unwin, 1986.